Four-Component Scattering Power Decomposition with Extended Volume Scattering Model

Akinobu Sato, Yoshio Yamaguchi, *Fellow, IEEE*, Gulab Singh, *Member, IEEE*, Sang-Eun Park, *Member, IEEE*

***Abstract*—In the three-component or four-component decompositions, polarimetric scattering properties and corresponding physical scattering models play essential roles for power decomposition. This letter proposes an improved four-component scattering power decomposition method that employs a suitable volume scattering model for single bounce or double bounce scattering in the polarimetric SAR image analysis. The cross-polarized *HV* component is created by both single bounce object (such as vegetation) and double bounce structures (such as oriented building blocks). It has been difficult to discriminate these two objects (vegetation against oriented buildings) in the decomposed images, since the *HV* component is assigned to the volume scattering due to vegetation only. We propose to extend the volume scattering model suited for two physical scattering models. It is shown that vegetation area and oriented urban building area are well discriminated compared to those resulting from implementation of the existing four-component scattering power decomposition.**

***Index Terms*—Polarimetric synthetic aperture radar (POLSAR), radar polarimetry, scattering power decomposition, volume scattering.**

I. INTRODUCTION

POLARIMETRIC scattering power decompositions based on physical scattering models have been attracting attention for target classification, detection, and land parameters retrieval for fully polarimetric SAR data analysis [1]-[4]. Model based approaches are simple and straightforward to implement on fully polarimetric SAR data take analyses [5], [6]. The three-component [3] and four-component decomposition [4]-[5] are well known in case of employing physical scattering models as typical targets classification and detection. There are 9 real independent polarimetric parameters in the coherency or covariance matrix for the most general scattering case. The four-component scattering power decomposition method [4] accounts for 6 terms out of 9 parameters by adding a helicity term to the three-component method [3]. After decomposing of total power into four components, it has been found that the method [4] has problems of overestimation in the volume scattering in urban areas and in negative power occurrence in the processing caused by a large cross-polarization component [5], [6]. Recently, Yamaguchi et al. [6] proposed a rotation method of the coherency matrix for more accurate polarimetric synthetic aperture radar (POLSAR) image decomposition and target classification. This is essentially identical with the deorientation method [7], [8], and the polarimetric orientation angle compensation method [9]. In addition, Arii et al. recently proposed an adaptive model-based decomposition method [10] to deal with volume scattering, which ensures non-negative power decomposition.

This rotation of coherency matrix significantly improved the decomposition results by minimizing the cross-polarized (*HV*) components and reduced the negative power occurrence in the surface scattering and the double bounce scattering components. The scattering powers are calculated easily, and are used to compose full color images with RGB color-coding; Red for the double bounce power, Green for the volume scattering power, and Blue for the surface scattering power, for which each color brightness is corresponding to the magnitude. They have been successfully applied to POLSAR image analysis because color-coded images are easier to understand, and because each color represents a specific scattering mechanism. This method accounts for 6 parameters out of 8 independent observable polarimetric parameters.
However, there still exists a problem of discrimination between vegetation and oriented buildings within the same volume scattering (Green) area. This ambiguity is caused by the assignment of the *HV* component. So far, the volume scattering power is evaluated by the *HV* component due to vegetation only in the existing methods [3]-[6]. To resolve the discrimination ambiguity, we have to assign the *HV* component whether it is created by vegetation (single bounce object) or by edges of oriented buildings (double bounce structures). In this letter, we propose to use a new volume scattering model that accounts for the *HV* component caused by double bounce structures versus vegetation scatter and to improve the four-component scattering power decomposition [6] for additional more accurate classification.

II. FOUR-COMPONENT SCATTERING DECOMPOSITION WITH ROTATION OF COHERENCY MATRIX

Once the scattering matrix [*S*] is acquired from fully polarimetric radar data sets, the Pauli vector can be defined as

$$\boldsymbol{k}_p = \frac{1}{\sqrt{2}} \begin{bmatrix} S_{HH} + S_{VV} \\ S_{HH} - S_{VV} \\ 2\, S_{HV} \end{bmatrix} \tag{1}$$

where S_{HH}, S_{VV}, and S_{HV} are elements of the scattering matrix, assuming the reciprocal condition of $S_{HV} = S_{VH}$.

Manuscript received May 10, 2011; revised June 21, 2011; accepted July 18, 2011. This work was supported by the grant of Space Sensing, Ministry of Education, Japan.

The authors are with Graduate School of Science and Technology, Niigata University, Japan. (e-mail: yamaguch@ ie.niigata-u.ac.jp).

The coherency matrix is given as

$$\langle [T] \rangle = \left\langle \boldsymbol{k}_p \boldsymbol{k}_p^{\dagger} \right\rangle = \begin{bmatrix} T_{11} & T_{12} & T_{13} \\ T_{21} & T_{22} & T_{23} \\ T_{31} & T_{32} & T_{33} \end{bmatrix} \quad (2)$$

where † denotes complex conjugation and transposition, and < > denotes ensemble average in an imaging window.

The coherency matrix after rotation by angle θ can be obtained as

$$\left\langle \left[T' \right] \right\rangle = [R(\theta)] \langle [T] \rangle [R(\theta)]^{\dagger} = \begin{bmatrix} T_{11}' & T_{12}' & T_{13}' \\ T_{21}' & T_{22}' & T_{23}' \\ T_{31}' & T_{32}' & T_{33}' \end{bmatrix} \quad (3)$$

where $$[R(\theta)] = \begin{bmatrix} 1 & 0 & 0 \\ 0 & \cos\theta & \sin\theta \\ 0 & -\sin\theta & \cos\theta \end{bmatrix} \quad (4)$$

The rotation angle θ *is determined so as to minimize the* T_{33} or equivalently the *HV component* [6].

$$\theta = \frac{1}{4} \tan^{-1} \left(\frac{2 \operatorname{Re}\{T_{23}\}}{T_{22} - T_{33}} \right) \quad (5)$$

The rotated measured coherency matrix $\langle [T'] \rangle$ is expanded into four sub-matrices which correspond to surface, double bounce, volume, and helix scattering mechanisms [6]

$$\langle [T'] \rangle = f_s \langle [T] \rangle_{surface} + f_d \langle [T] \rangle_{double} + f_v \langle [T] \rangle_{vol} + f_c \langle [T] \rangle_{helix} \quad (6)$$

where f_s, f_d, f_v and f_c are coefficients to be determined. $\langle [T] \rangle_{surface}$, $\langle [T] \rangle_{double}$, $\langle [T] \rangle_{vol}$ and $\langle [T] \rangle_{helix}$ are expansion matrices corresponding to the surface, double bounce, volume, and helix scattering, respectively[2]-[5].

The expansion matrix for the surface scattering is

$$\langle [T] \rangle_{surface} = \begin{bmatrix} 1 & \beta^* & 0 \\ \beta & |\beta|^2 & 0 \\ 0 & 0 & 0 \end{bmatrix}, \quad |\beta| < 1 \quad (7)$$

The expansion matrix for the double bounce scattering is

$$\langle [T] \rangle_{bouble} = \begin{bmatrix} |\alpha|^2 & \alpha & 0 \\ \alpha^* & 1 & 0 \\ 0 & 0 & 0 \end{bmatrix}, \quad |\alpha| < 1 \quad (8)$$

For the volume scattering model, we must confirm from the experimental evidence that $\operatorname{Re}\{\langle S_{HH} S_{VV}^* \rangle\} > 0$ is corresponding to the surface scattering. Under the condition $\operatorname{Re}\{\langle S_{HH} S_{VV}^* \rangle\} > 0$, the *HV* component is assigned to a cloud of randomly oriented dipole scatterers such as vegetation. We choose one of the following matrices according to the magnitude balance of $\langle |S_{HH}|^2 \rangle$ and $\langle |S_{VV}|^2 \rangle$

For $10 \log \left(\langle |S_{VV}|^2 \rangle / \langle |S_{HH}|^2 \rangle \right) > 2\ dB$

$$\langle [T] \rangle_{vol}^{dipole} = \frac{1}{30} \begin{bmatrix} 15 & -5 & 0 \\ -5 & 7 & 0 \\ 0 & 0 & 8 \end{bmatrix} \quad (9)$$

For $\left| 10 \log \left(\langle |S_{VV}|^2 \rangle / \langle |S_{HH}|^2 \rangle \right) \right| < 2\ dB$

$$\langle [T] \rangle_{vol}^{dipole} = \frac{1}{4} \begin{bmatrix} 2 & 0 & 0 \\ 0 & 1 & 0 \\ 0 & 0 & 1 \end{bmatrix} \quad (10)$$

For $10 \log \left(\langle |S_{VV}|^2 \rangle / \langle |S_{HH}|^2 \rangle \right) < -2\ dB$

$$\langle [T] \rangle_{vol}^{dipole} = \frac{1}{30} \begin{bmatrix} 15 & 5 & 0 \\ 5 & 7 & 0 \\ 0 & 0 & 8 \end{bmatrix} \quad (11)$$

However, for the case of $\operatorname{Re}\{\langle S_{HH} S_{VV}^* \rangle\} < 0$, we have to use a different alternate expansion matrix as shown in the next section.

Helix scattering power is equivalent to circular polarization power. This term appears in urban and mountainous regions for L-band data. The helix scattering expansion matrix is

$$\langle [T] \rangle_{helix} = \frac{1}{2} \begin{bmatrix} 0 & 0 & 0 \\ 0 & 1 & \pm j \\ 0 & \mp j & 1 \end{bmatrix} \quad (12)$$

The corresponding scattering powers (the surface scattering power P_s, the double bounce scattering P_d, the volume scattering power P_v and the helix scattering power P_c) are directly obtained from the expansion coefficients by applying the decomposition algorithm. Details of this method are given in [6].

III. NEW FOUR-COMPONENT SCATTERING POWER DECOMPOSITION

In this section a new four-component scattering power decomposition method is explained using a new volume scattering model.

A. New Expansion Matrix for Dihedral Scattering

The experimental evidence indicates that $\operatorname{Re}\{\langle S_{HH} S_{VV}^* \rangle\} < 0$ corresponds to the double bounce scattering case. This situation typically occurs for man-made objects with right angle structures such as building walls and roads, and river surfaces and bridges orthogonal to radar illumination. We call this kind of structure dihedral structures. When the directions of the main surface of buildings are oriented with respect to radar illumination, the *HV* component is generated and becomes a relatively large term in the acquired scattering matrix. We must consider this physical situation in more detail and must incorporate the *HV* component by the oriented dihedral structures for more accurate modeling.

Since the rotation of coherency matrix minimizes the *HV* component [6], most of the orientations of dihedral structures

are centered about 0 degree with respect to the direction of radar illumination after the rotation (3). In order to derive a new expansion coherency matrix for the *HV* component, we implement ensemble averaging of dihedral corner reflectors using a probability density function $p(\theta)$ with its peak at 0 degree, as shown in Fig. 1.

$$p(\theta) = \frac{1}{2}\cos\theta \qquad for \ -\frac{\pi}{2} < \theta < \frac{\pi}{2} \tag{13}$$

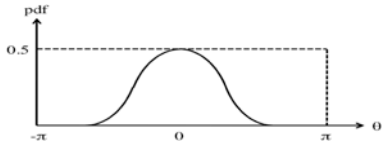

Fig.1. Probability density function

The theoretical ensemble matrix for a dihedral corner reflector can be derived from

$$\langle [T(\theta)] \rangle = \int_{-\pi/2}^{\pi/2} [T(\theta)] p(\theta) d\theta \tag{14}$$

yielding,

$$\langle [T] \rangle_{vol}^{dihedral} = \frac{1}{15}\begin{bmatrix} 0 & 0 & 0 \\ 0 & 7 & 0 \\ 0 & 0 & 8 \end{bmatrix} \tag{15}$$

This matrix was derived using (3) for dihedral in a similar way explained in [4] and was set so that the Trace becomes unity. We use this matrix as a new volume scattering expansion matrix that accounts for the *HV* component for dihedral structures.

B. Branch Condition

After rotation of coherency matrix, we first discriminate the scattering mechanism using the sign of $\mathrm{Re}\{\langle S_{HH} S_{VV}^{*} \rangle\}$. It is known from the experimental evidence that the double scattering by dihedrals cause the parameter $\mathrm{Re}\{\langle S_{HH} S_{VV}^{*} \rangle\}$ to be negative. On the other hand, non-dihedral structure causes $\mathrm{Re}\{\langle S_{HH} S_{VV}^{*} \rangle\} > 0$. These relations can be explained in more detail by rigorously using the covariance matrix formulation [4]. By the expansion of the C_{13} component for randomly distributed dipoles [4], we can derive the equation as follows:

$$\mathrm{Re}\{f_s \beta + f_d \alpha^{*}\} + \frac{1}{8} f_v - \frac{1}{4} f_c = \mathrm{Re}\{\langle S_{HH} S_{VV}^{*} \rangle\} \tag{16}$$

This equation can be re-arranged to

$$C_1 = 2\,\mathrm{Re}\{f_s \beta + f_d \alpha^{*}\} = 2\,\mathrm{Re}\{\langle S_{HH} S_{VV}^{*} \rangle\} + \frac{1}{2} f_c = T_{11}^{'} - T_{22}^{'} + \frac{1}{2} f_c \tag{17}$$

We have omitted the term $\frac{1}{8} f_v$ in the above equation (17) because the volume scattering coefficient is not decided at this stage. The sign of (17) determines the dominant scattering mechanism, i.e., surface scattering versus double bounce scattering. According to the sign of C_1, we assign the volume scattering (the *HV* component) to surface scattering (vegetation) or double bounce (oriented dihedral structure) according to the following condition:

$$C_1 = T_{11}^{'} - T_{22}^{'} + \frac{1}{2} f_c > 0, \ \textit{volume scattering by vegetation} \tag{18}$$

$$C_1 = T_{11}^{'} - T_{22}^{'} + \frac{1}{2} f_c \le 0, \ \textit{volume scattering by dihedral} \tag{19}$$

It should be noted that (18) and (19) are the first-stage criteria. It happens that (19) assigns the volume scattering as dihedral scattering when double bounce by forest trunk and ground is too strong in vegetation area. However, it is easy to recognize vegetation scattering area in this case because the tree trunk and ground scattering (double bounce) points appear randomly and sparsely in the surrounding area and the volume scattering dominates in the final decomposed forest image.

To check the validity of the criteria, L-band Pi-SAR data sets have been analyzed. These Pi-SAR data sets were acquired over Niigata University and surrounding area. Fig. 2(a) shows the optical Google Earth image over the area. Fig 2(b) represents the C_1 binary image of Pi-SAR data, corresponding to Fig. 2(a). We can clearly see $C_1 > 0$ in pine forest areas in the upper part of Fig.2 (a), and $C_1 \le 0$ in orthogonal urban areas (middle left) to radar illumination direction. On the other hand, we see mixture of $C_1 > 0$ and $C_1 \le 0$ in oriented urban area (right). This result confirms the validity of the criteria, which will be applied in new decomposition method.

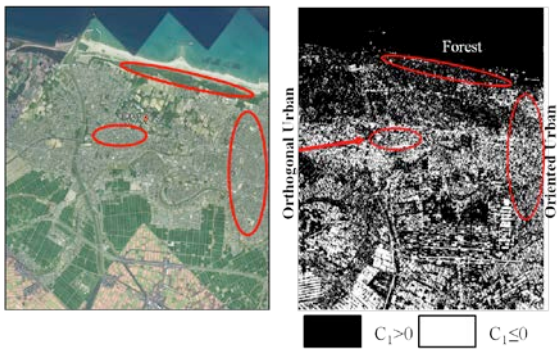

(a) (b)

Fig. 2. (a) Google Earth Optical image (b) C_1 binary image of Pi-SAR data over Niigata University and srounding area derived by eq. (17).

C. New four-component scattering power decomposition

New decomposition can be explained in eq. (20) and in Fig. 3 by using the volume scattering component from vegetation and/or oriented dihedral structures.

$$\left\langle \left[T^{'} \right] \right\rangle = f_s \langle [T] \rangle_{surface} + f_d \langle [T] \rangle_{double} + f_c \langle [T] \rangle_{helix} + \begin{cases} f_v \langle [T] \rangle_{vol}^{dipole} & for \ C_1 > 0 \\ f_{vd} \langle [T] \rangle_{vol}^{dihedral} & for \ C_1 \le 0 \end{cases} \tag{20}$$

where f_s, f_d, f_v, f_{vd} and f_c are coefficients to be determined. $\langle [T] \rangle_{surface}$, $\langle [T] \rangle_{double}$ and $\langle [T] \rangle_{helix}$ are expansion matrices

corresponding to surface, double bounce, and helix scattering, respectively. $\langle[T]\rangle_{vol}^{dihedral}$ and $\langle[T]\rangle_{vol}^{dipole}$ are the volume scattering matrices for oriented dihedral structure and wire (ensemble average of dipole), respectively.

The total power (TP) decomposes into surface scattering power P_s, double bounce scattering power P_d, volume scattering power P_v, from dipole and/or oriented dihedral and helix (P_c), as shown in Fig. 3.

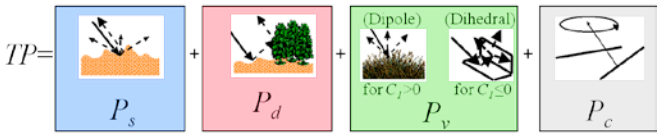

Fig. 3 New four-component scattering mechanism with rotation of coherency matrix.

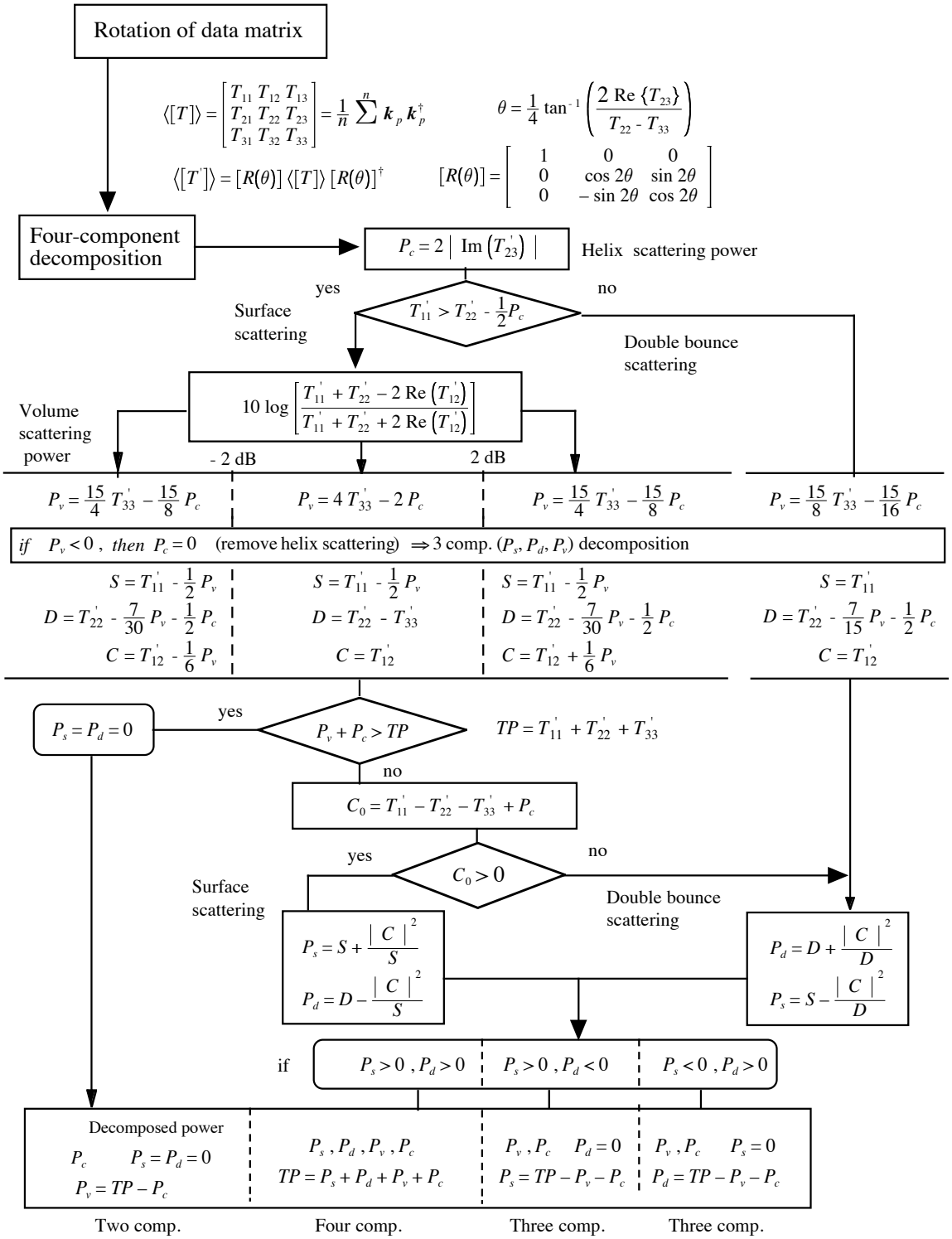

Fig.4. Four-component decomposition with a rotation about line of sight to set Re(T23)=0 and the remaining *HV* contribution due to scattering from either a dihedral or a dipole distribution.

D.Decomposition Algorithm

The new decomposition algorithm is shown in Fig. 4. First important step is the rotation of coherency matrix to minimize the *HV* component before the decomposition. It should be noted that (5) assumes arctan2 for obtaining the rotation angle in the computer algorithm. This rotation forces real-part of T23 to be zero, so that it ensures a reduction of the number of independent polarimetric parameters from 9 to 8. Then we check the sign of C_1 to assign the prevalent scattering mechanism. Once assigned to double bounce scattering, we use a new expansion matrix (15) for volume scattering. Since most of double bounce structures are faced to radar illumination direction by implementation of the rotation of coherency matrix, the *HV* component comes from this dihedral structure.

On the other hand, if surface scattering is assigned, we use the same decomposition procedure as derived in [6]. Once the character of volume scattering power has been determined, it is possible to critically determine the dominant scattering mechanism within the volume scattering generated due dipoles at this stage. We check the second branch condition using (16) to confirm the scattering mechanism again.

$$2\,\mathrm{Re}\{f_s\,\beta + f_d\,\alpha^*\} = 2\,\mathrm{Re}\{\langle S_{HH}S_{VV}^*\rangle\} - 2\langle|S_{HV}|^2\rangle + P_c \quad (21)$$

This expression is equivalent to (22) in terms of coherency matrix elements

$$C_0 = T_{11}' - T_{22}' - T_{33}' + P_c \quad (22)$$

The sign of C_0 determines the dominant scattering mechanism precisely within the volume scattering.

$$\begin{aligned} &C_0 > 0 \ : \text{surface scattering,} \\ &C_0 \le 0 \ : \text{double bounce scattering.} \end{aligned} \quad (23)$$

All of these physical branch conditions are included in a flowchart of the decomposition algorithm in Fig. 4.

IV. Decomposition Results

Both existing [6] (four-component decomposition with rotation of coherency matrix) and the proposed procedures of decomposition methods have been applied to Pi-SAR images collected over Niigata University and environs. The volume scattering component due to [6] and the proposed method are shown in Fig. 5. Using the proposed extended volume scattering model, significant reduction of volume scattering can be seen in dihedral structures (oriented urban and orthogonal urban areas) compared to the method developed in [6]. This fact serves for regulating the overestimation problem of the volume scattering in urban areas. On the other hand, the volume scattering remains almost the same in forested vegetation areas. Therefore, the proposed dihedral volume scattering model is expected to contribute for improving the decomposition accuracy in volume scattering.

Fig. 6 shows the decomposed color-coded composite images by both the existing and the proposed new methods for the sake of comparison. The differences are clearly seen between images (a) and (b). We can see more "Red" in (b) more than in (a). This indicates that the dihedral structures are enhanced, while "Green" caused by volume scattering within dihedral structures are reduced. In order to examine these results quantitatively, the decomposed power profiles along a transect over sandy ground, forest and urban area (white line A in Figs. 6 and 7 (a)) are shown in Fig. 7 (b) and (c). Dashed lines on the Fig.7 (b) and (c) show the boundaries of sand, forest and urban areas. It is seen that the proposed method does not change the amount of volume scattering in sandy and forest area as compared to method [6]. The presented new method reduces the amount of volume scattering power in urban areas where many residential houses exist as shown in red circle of Fig.7(b) and (c).

This new four-component decomposition scheme is also applied to many ALOS-PALSAR quad-pol. images for verifying the correct implementation of this scheme. Fig. 8 shows San Francisco image (Scene ID: ALPSRP276160750) acquired on April 1, 2011, and compares the method derived in [6] with the new method. The interesting observation relates to the 40 degree oriented urban area and a bridge on the right part of images. The green color of the oriented urban area in (a) is suppressed in (b). We can recognize that this area is made up of man-made structures because of so many scattered red spots. The sharpness of the upper bridge is excellent in (b), where we can see three lines indicating single bounce, double bounce, and triple bounce very clearly [7]. The green area within in park (center left) remains almost the same, while the purple red urban blocks and roads around the park in (b) are displayed more clearly.

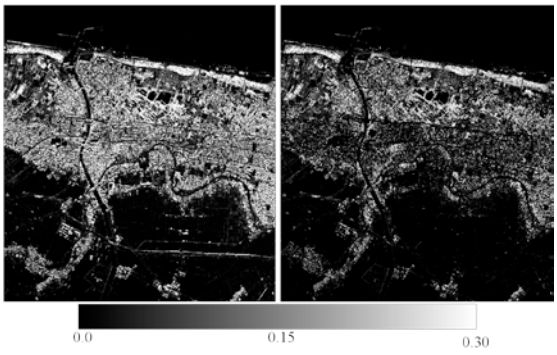

Fig.5 (a) Volume scattering component derived from [6], (b) volume scattering component derived by the new method.

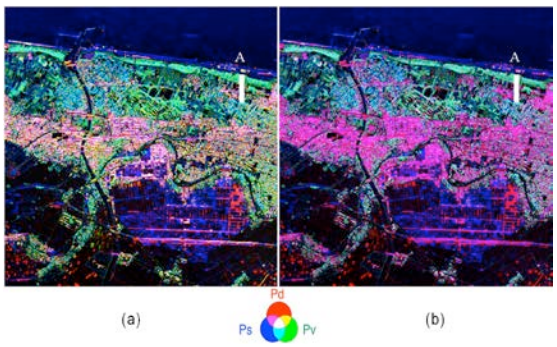

Fig. 6 Color-coded decomposed image of the Niigata University area by L-band Pi-SAR polarimetric data. (a) by existing method [6], (b) by proposed method

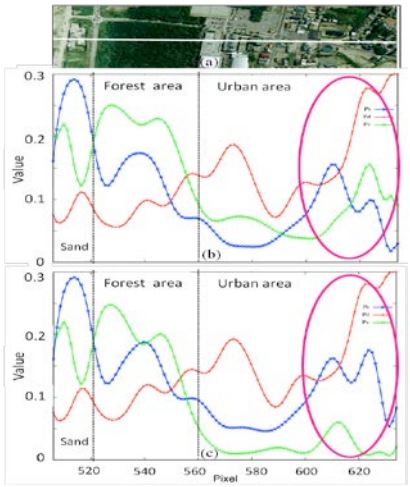

Fig.7. (a) Photo by Google Earth, (b) Profile of scattering components derived based on existing method [6], (c) profile of scattering components derived based on proposed method.

V. Conclusion

In this letter, we proposed a new volume scattering model that accounts for the *HV* component caused by double bounce structures. This model better describes the *HV* component induced by rotated dihedral scattering and reduces the volume scattering power and enhances the double bounce scattering power within man-made structures, leading to an improvement in the four- component scattering power decomposition. This decomposition method accounts for 6 terms out of 8 real independent polarimetric parameters for the most general scattering case with a help of rotation of coherency matrix. The decomposition results are in good agreement with Google Earth optical images.

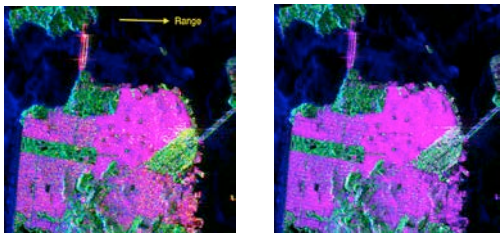

(a) (b)

Fig. 8 Color-coded decomposed image of San Francisco on April 1, 2011, acquired with ALOS-PALSAR PLR mode. (a) method [6], (b) proposed method

Acknowledgment

The authors are grateful to JAXA for providing L-band Pi-SAR and ALOS-PALSAR sets. We thank Dr. Wolfgang –M. Boerner, Professor Emeritus, University of Illinois at Chicago, for checking the manuscript.

References

[1] J. S. Lee and T. Ainsworth, "An overview of recent advances in polarimetric SAR information extraction: algorithms and applications," *Proc. of IGARSS 2010*, pp. 851-854, 2010.

[2] J. S. Lee and E. Pottier, *Polarimetric radar imaging from basics to applications*, CRC Press, 2009.

[3] A. Freeman and S. Durden, "A three-component scattering model for polarimetric SAR data," *IEEE Trans. Geosci. Remote Sens.,* vol. 36, no. 3, pp. 963-973, May 1998.

[4] Y. Yamaguchi, T. Moriyama, M. Ishido, and H. Yamada, "Four-component scattering model for polarimetric SAR image decomposition," *IEEE Trans. Geosci. Remote Sens.,* vol. 43, no. 8, pp. 1699-1706, Aug. 2005.

[5] Y. Yajima, Y. Yamaguchi, R. Sato, H. Yamada, and W.-M. Boerner, "POLSAR image analysis of wetlands using a modified four-component scattering power decomposition," *IEEE Trans. Geosci. Remote Sens.,* vol. 46, no. 6, pp. 1667-1773, June 2008.

[6] Y. Yamaguchi, A. Sato, W.-M. Boerner, R. Sato, and H. Yamada, "Four-component scattering power decomposition with rotation of coherency matrix," *IEEE Trans. Geosci. Remote Sens.,* vol. 49, no. 7, July 2011 (in press).

[7] F. Xu, and Y. Q. Jin, "Deorientation theory of polarimetric scattering targets and application to terrain surface classification," *IEEE Trans. Geosci. Remote Sens.*, vol. 43, no. 10, pp. 2351-2364, Oct. 2005.

[8] W. An, Y. Cui, and J. Yang, "Three-component model-based decomposition for polarimetric SAR data," *IEEE Trans. Geosci. Remote Sens.*, vol. 48, no. 6, pp. 2732 – 2739, June 2010.

[9] J. S. Lee and T. Ainsworth, "The effect of orientation angle compensation on coherency matrix and polarimetric target decompositions," *IEEE Trans. Geosci. Remote Sens.*, vol. 49, no. 1, pp. 53-64, Jan. 2011.

[10] M. Arii, J. J. van Zyl, and Y. J. Kim, "Adaptive model-based decomposition of polarimetric SAR covariance matrices," *IEEE Trans. Geosci. Remote Sens.*, vol. 49, no. 3, pp. 1104 – 1113, Mar. 2011.